


**Interlayer polarizability in twisted bilayer graphene quantum dots**Xian Wang,<sup>1</sup> Li Zhang,<sup>1</sup> Shengping Yu,<sup>2</sup> Mingli Yang<sup>1,\*</sup> and Koblar Alan Jackson<sup>3,†</sup><sup>1</sup>*Institute of Atomic and Molecular Physics, Key Laboratory of High Energy Density Physics of Ministry of Education, Sichuan University, Chengdu 610065, China*<sup>2</sup>*School of Chemistry and Environment, Southwest Minzu University, Chengdu 610041, China*<sup>3</sup>*Department of Physics, Central Michigan University, Mt. Pleasant, Michigan 48859, USA* (Received 6 June 2021; revised 22 September 2021; accepted 23 September 2021; published 7 October 2021)

Many of the intriguing properties of bilayer graphene (BLG) are related to interlayer electronic coupling. Since this coupling is sensitive to an applied electric field perpendicular to the layers, we develop a strategy for determining interlayer coupling by decomposing the total electric dipole polarizability, which measures the response of electrons to applied fields, into site-specific contributions and consequently the intralayer and interlayer components. The interlayer polarizability is evaluated from field-induced electron density variations computed with a first-principles approach for twisted BLG quantum dots (QDs). Changes in interlayer polarizability dominate the polarizability variation with twist angle. In addition to the well-recognized strong coupling in the Bernal stackings, enhanced coupling is revealed for the structures at small and size-dependent twist angles when AB stacking first appears in the outermost shell of the QD. The values of these magic angles depend on the QD size. This paper not only provides an approach for measuring interlayer coupling strength but also indicates the existence of strong interlayer coupling even at small twist angles, which could be important for understanding the properties of twisted BLG.

DOI: [10.1103/PhysRevB.104.155411](https://doi.org/10.1103/PhysRevB.104.155411)**I. INTRODUCTION**

Graphene and graphene quantum dots (GQDs) have good potential for use in quantum information applications owing to their weak spin-orbit, hyperfine interaction and long expected spin lifetime [1–4]. These applications, however, rely on a controlled confinement and density of electrons and holes [5–11]. Carrier confinement has been realized in bilayer graphene (BLG) quantum dots (QDs) with opened band gaps [6,7]. Moreover, the band gaps can be further tuned by applying an external electric field perpendicular to the graphene planes [6–11,12–19]. The barrier to interlayer electron tunneling is then tunable to localize a specified number of electrons/holes, which is one of the platforms for spin qubits [8–10]. The direction and strength of the applied electric field has great influence on the interlayer coupling and consequently on the tunnel barrier. Modulation of the interlayer coupling strength is an effective way to tune the confinement of carriers in the BLG-based devices.

In addition to applied electric fields, interlayer stacking order has also been used to tune the interlayer coupling in BLG. Sagar *et al.* [20] identified strong interlayer coupling in the full-AB (Bernal) stacking in BLG, which is, however, decoupled in the misoriented stacking, accompanied by a dramatic resistance increase in scanning photocurrent microscopy measurements. Significant interlayer conductance was observed in turbostratic graphene, which was attributed

to phonon scattering processes [21]. The interlayer contact conductance is twist angle dependent owing to the overall contribution of local interfacial carrier density and tunneling barrier [22]. Abnormal conductivity in low-angle twisted BLG (TBG) was observed and attributed to the reduction in average carrier density [23]. Therefore, interlayer stacking provides an additional degree of freedom to tune the interlayer interaction. While most concerns focused on the AB stacking that requires a large twist angle, on the other hand, a variety of intriguing properties including superconductivity [24,25], correlated insulators [26], and van Hove singularities [27,28] have been reported for BLG at small twist angles. Rotations between the two layers lead to various stacking patterns that are responsible for these phenomena not observed in untwisted BLG.

Since external field and interlayer twist have been separately used to tune the interlayer interaction of BLG, it is expected that even better control could be reached by their combination. Advances in experimental techniques make it possible to grow multilayer graphene with single-layer precision [29], to carve two-dimensional graphene into zero-dimensional QDs [30,31], to apply an external electric field in a gated hexagonal boron nitride (hBN)-BLG-hBN heterostructure device [32,33], and to twist one of the layers at a specified angle [34]. In almost all the advances in BLG and its QDs, interlayer interaction plays a key role in their intriguing properties. While interlayer coupling is clearly important, quantitative measures of its strength are lacking, especially in cases involving external fields.

Polarizability, measuring the response of electrons to an external field, is clearly an appropriate quantity for exploring the field-induced response of BLG. The challenge is how to

\*myang@scu.edu.cn

†jacks1ka@cmich.edu

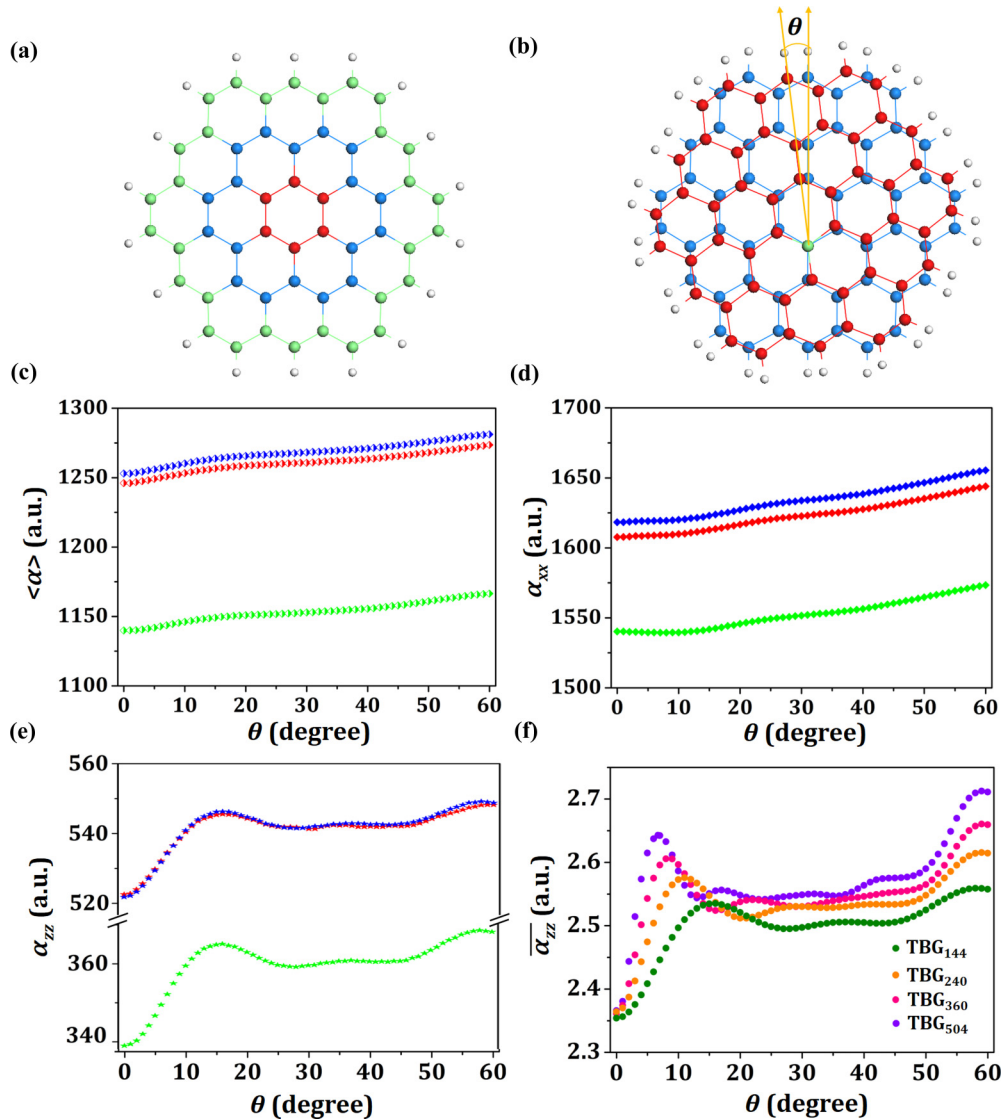


FIG. 1. (a) Monolayer graphene quantum dot (QD) with three shells. (b) Twisted bilayer graphene (TBG) QD with a twisting angle of  $\theta$ . (c)  $\langle \alpha \rangle$ , (d)  $\alpha_{xx}$ , and (e)  $\alpha_{zz}$  vs twist angle using CAM-B3LYP/6-31G(d,p) (in green),  $\omega$ B97XD/6-31++G(d,p) (in red), and CAM-B3LYP/6-31++G(d,p) (in blue). (f)  $\alpha_{zz}/N$  computed with CAM-B3LYP/6-31G(d,p).  $N$  is the number of atoms in the QD.

define the contribution to the polarizability from interlayer interactions. In this paper, a first-principles, site-specific polarizability method is used to evaluate interlayer polarizability in TBG QDs and to study its variation with twist angle. Our results confirm the previously reported [20–28] strong interlayer coupling, which occurs either in AB-stacked QDs or moiré superlattices in TBG, and reveal that strong coupling also occurs in the finite-sized QD structures at small, size-dependent twist angles.

## II. METHODS

The TBG QD model consists of two layers parallel to the  $xy$  plane with a separation of 0.334 nm [35–37]. Four models, TBG<sub>144</sub>, TBG<sub>240</sub>, TBG<sub>360</sub>, and TBG<sub>504</sub> of 1.24, 1.73, 2.22, and 2.71 nm in diameter, respectively, are constructed with their carbon atoms grouped into 3–6 shells [see Fig. 1(a)], respectively. The monolayer QD consisting of 54 carbon atoms and

18 terminal hydrogen atoms that was previously characterized in experiments [38] forms one layer of TBG<sub>144</sub>. Relative to the fixed lower layer, the upper layer of the QD is rotated about one of the C atoms in the central six-membered ring by an angle  $\theta$  [see Fig. 1(b)]. Rotations about the hexagonal centers are also studied for the four systems.

These structures are then studied within a density functional theory framework using the GAUSSIAN16 package [39]. The functionals CAM-B3LYP [40] and  $\omega$ B97XD [41], including long-range and van der Waals (vdW) corrections are used, which are pivotal for an appropriate description of the interlayer coupling in vdW heterojunctions. These two functionals are used respectively with the standard basis sets 6-31G(d,p) and 6-31++G(d,p) [42] augmented by one  $s$ -type diffuse function on hydrogen atoms and one  $p$ -type diffuse function on carbon atoms. The polarizability is computed with a finite field (FF) method [43] based on the total and atomic dipole moments. The atomic dipole moments and net charges are

evaluated with a Hirshfield partitioning approach [44,45]. The applied field in the FF approach is set to 0.001 a.u., a strength that provides numerical stability while avoiding contamination from higher-order contributions to the polarizability.

### III. RESULTS AND DISCUSSION

The relative energy of the QD structures varies with twist angle. Taking the TBG<sub>144</sub> as an example, the full-AA stacking at  $\theta = 0^\circ$  has the highest energy, which decreases rapidly with the twist angle, and reaches the lowest point in the full-AB stacking at  $\theta = 60^\circ$ , as illustrated in Fig. S1 in the Supplemental Material [46]. Figure 1(c) shows the variation of the isotropic polarizability  $\langle\alpha\rangle = (\alpha_{xx} + \alpha_{yy} + \alpha_{zz})/3$  of TBG<sub>144</sub> with rotation. The functionals CAM-B3LYP and  $\omega$ B97XD, including long-range and vdW corrections, produce similar results when the 6-31++G(d,p) basis set is employed. Excluding diffuse basis functions reduces the calculated polarizability but gives the same trend. Here,  $\langle\alpha\rangle$  has its minimum at  $\theta = 0^\circ$  and increases steadily with the rotation. Moreover, all components,  $\alpha_{xx}$  and  $\alpha_{zz}$  increase when  $\theta$  departs from  $0^\circ$  [see Figs. 1(d) and 1(e)], but their rates of increase are very different. Note that  $\alpha_{yy} \approx \alpha_{xx}$  due to symmetry. Only a small relative increase of  $\sim 2\%$  is noted for  $\alpha_{xx}$ , while  $\alpha_{zz}$  increases by  $\sim 5\%$ . Similar variations in  $\alpha_{zz}$  are noted in Fig. 1(f) for the three larger TBG<sub>N</sub>. The enhanced  $\alpha_{zz}$  hints that electron rearrangement in the  $z$  direction is more significantly affected by the applied field. Rotations about the hexagonal centers produce similar variations, as presented in Fig. S2 in the Supplemental Material [46]. Moreover, similar  $\alpha_{zz}$  variations are obtained if one uses the equilibrium interlayer distances for each twist angle instead of the fixed one (0.334 nm; see Fig. S3 in the Supplemental Material [46]).

Here,  $\alpha_{zz}$  increases rapidly at small  $\theta$  and reaches the first local maximum at  $\sim 16^\circ$ ,  $11^\circ$ ,  $8^\circ$ , and  $6.8^\circ$  ( $\theta_p$ ) for the four models, respectively. Thereafter,  $\alpha_{zz}$  remains close to the maximum value until  $\theta$  nears  $60^\circ$ . As indicated by  $\alpha_{zz}$ , the interlayer coupling is weakest at  $\theta = 0^\circ$  but enhanced upon rotation. Such rotation-dependent properties have been reported for TBG in many studies, including superconductivity at  $\theta = 1.1^\circ$  [24], van Hove singularities at  $0.79^\circ$  [28], pseudo-Landau levels at  $0.48^\circ$  [47], and higher-order topological insulators at large commensurate angles [48]. All these angle-dependent properties are correlated to specific moiré patterns that correspond to different interlayer stackings. While magic angles in infinite TBG have been attributed to their flat low-energy bands and strong electron correlation [24–26], it remains unclear how the magic angles for those  $\alpha_{zz}$  maxima occur in finite-sized QDs. We explore the twist-angle-dependent interlayer coupling below by extracting the interlayer polarizability from the total polarizability.

Polarization in the  $z$  direction has two origins, intralayer and interlayer [see Fig. 2(a)]. The intralayer part comes from electron redistribution between the upper and lower sides of each layer separately. The interlayer part involves electron transfer between them. We developed a polarizability partitioning scheme [49] that decomposes the total polarizability into site-specific contributions, making it possible to distinguish the intralayer and interlayer counterparts of the polarizability. This scheme has been used to study the evo-

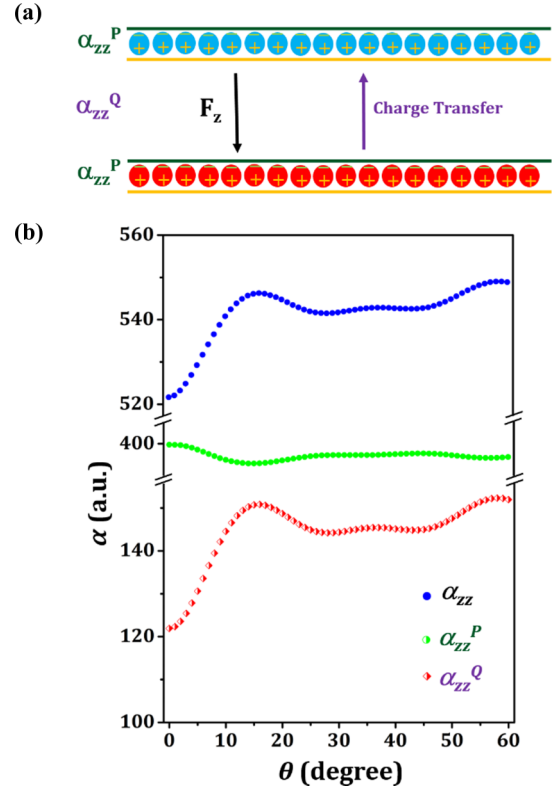


FIG. 2. (a) Diagram of intralayer and interlayer polarizability.  $F_z$  denotes the applied field in the  $z$  direction. (b)  $\alpha_{zz}$  and its dipole and charge-transfer parts of twisted bilayer graphene TBG<sub>144</sub>.

lution of dielectric behavior in atomic clusters [50–52]. The QD is divided into upper and lower parts with respect to the  $xy$  plane. One has

$$\alpha_{zz} = \alpha_{zz,U}^P + \alpha_{zz,L}^P + \alpha_{zz}^Q, \quad (1)$$

where  $\alpha_{zz}^P$  and  $\alpha_{zz}^Q$  denote intralayer and interlayer polarizability, respectively, and  $U$  and  $L$  denote the upper and lower layers, respectively. The intralayer and interlayer polarizability are evaluated by

$$\alpha_{zz,U(L)}^{P(Q)} = \left. \frac{d[\sum_{i \in U(L)} \mu_{i,z}^{P(Q)}]}{dF_z} \right|_{F_z \rightarrow 0}, \quad (2)$$

where

$$\mu_{i,z}^P = \int (r_z - r_{i,z}^0) w_i(\mathbf{r}) \rho(\mathbf{r}) d\mathbf{r}, \quad (3)$$

$$w_i(\mathbf{r}) = \frac{\rho_i^0(\mathbf{r})}{\sum_i \rho_i^0(\mathbf{r})}, \quad (4)$$

and

$$\mu_{i,z}^Q = r_{i,z}^0 q_i = r_{i,z}^0 \int w_i(\mathbf{r}) \rho(\mathbf{r}) d\mathbf{r}, \quad (5)$$

where  $\rho(\mathbf{r})$  is the electron density at  $\mathbf{r}$ ,  $r_i^0$  is the location of atom  $i$ , and  $q_i$  is the net atomic charge. The electron density is decomposed into atomic contributions using a Hirshfield approach [44,45], in which the density is partitioned

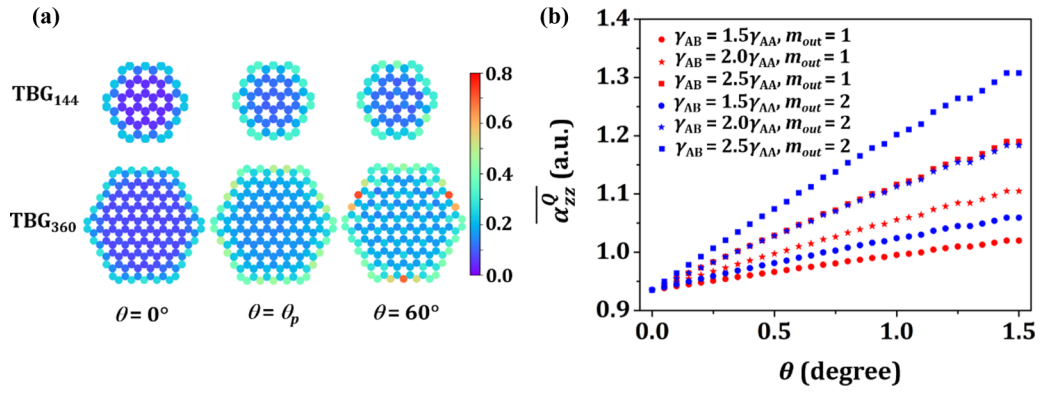


FIG. 3. (a) Atomic  $\gamma$  value of twisted bilayer graphene (TBG) quantum dots (QDs) at  $\theta = 0^\circ$ ,  $\theta_p$ , and  $60^\circ$ . (b) Predicted  $\overline{\alpha_{zz}^Q}$  of TBG as a function of twisting angle.  $m_{out}$  is the number of shells in AB stacking.

according to a weight factor ( $w_i$ ) evaluated from the premolecular density  $\rho_i^0(\mathbf{r})$ , of individual atoms.

The computed site-specific components,  $\alpha_{zz}^Q$  and  $\alpha_{zz}^P$  of TBG<sub>144</sub> are presented in Fig. 2(b). Here,  $\alpha_{zz}^P$  varies by  $\sim 1\%$ , while  $\alpha_{zz}^Q$  has large relative variations of  $\sim 25\%$  as  $\theta$  rotates from  $0^\circ$  to  $60^\circ$ . Because of this,  $\alpha_{zz}$  follows the same pattern of variation as  $\alpha_{zz}^Q$ . Here,  $\alpha_{zz}^Q$  increases rapidly at small  $\theta$ , reaches its first peak at  $16^\circ$ , drops slightly, and then increases gradually until reaching the next peak at  $58^\circ$ .

The interlayer polarizability clearly depends strongly on the twist angle, which alters the relative locations of carbon atoms between the two layers. All carbon atoms are in an AA stacking pattern in which every atom in the top layer is right above an atom in the bottom layer at  $\theta = 0^\circ$ . All atoms in one layer except the central one on the rotation axis are displaced relative to the atoms in the other layer when the rotation starts. At  $\theta_p = 16^\circ$ ,  $11^\circ$ ,  $8^\circ$ , and  $6.8^\circ$ , some carbon atoms in the outermost shells are roughly above the center of six-membered rings in the opposite layer, respectively, which is referred to as the AB stacking pattern. At  $\theta = 60^\circ$ , the atoms in all shells are found in the AB pattern. For the other angles, the atoms in the two layers are in intermediate stacking between AA and AB. The fluctuations in interlayer conductance and transport between  $0^\circ$  and  $60^\circ$  have been characterized in previous experiments and computations [22,23,53,54]. Our calculations address the fluctuations in interlayer polarizability, and the number of peaks increases with QD size. The relative importance of these three patterns (AA, AB, and their intermediate stackings) varies with increasing  $\theta$ , contributing differently to interlayer polarizability. The maximum  $\alpha_{zz}^Q$  appears in the Bernal structure near  $\theta = 60^\circ$ . It is apparent that the enhanced interlayer polarizability is related to AB stacking in the twisted structures. Authors of some studies [20–22] have recognized the strong interlayer coupling in the Bernal stacking of graphene QDs but claimed a weaker coupling in the other misoriented structures.

Equations (2)–(5) allow us to decompose the interlayer polarization into atomic contributions. Since  $\mu_{i,z}^Q$  is coordinate dependent, we define  $\gamma = \delta q^i / \delta F_z$ , which denotes the variation of the net atomic charge induced by an external field. Here,  $\gamma$  is then the decisive term in  $\alpha_{zz}^Q$  and used to measure the atomic contribution to interlayer polarizability. The atomic

$\gamma$  values at selected angles ( $0^\circ$ ,  $\theta_p$ , and  $60^\circ$ ) of TBG<sub>144</sub> and TBG<sub>360</sub> are presented in Fig. 3(a). Atoms in the same/different shells have similar/different  $\gamma$  values. Similar trends are noted for the other rotation angles. Here,  $\gamma$  tends to increase from the inner to the outer shell, its magnitude varies in a similar way with the rotation angle in each shell. The  $\gamma$  variations indicate that two factors influence the magnitude of  $\gamma$ , the distance of the atom from the center, and its stacking pattern relative to the six-membered ring in the other layer. Atoms closer to the AB pattern and/or atoms in the outer shells tend to possess larger  $\gamma$  values. In the QD model, the atoms near the edge are terminated by H atoms. This is likely to affect the specific value of  $\gamma$  for atoms in the outer shell, but we do not expect these changes to significantly change the picture described here.

The changing  $\gamma$  values for atoms from inner to outer shells indicate a dependence of their displacements upon rotation, which clearly correspond to deviations from the AA structure. The atoms farther from the central atom have larger displacements and approach closer to AB stacking within a moiré period. The mixing of AA, AB, and their intermediate stackings makes the  $\gamma$  dependence on the stacking pattern complex. Figure 3(a) depicts the  $\gamma$  variations for atoms at different locations. The  $\gamma$  values are small and similar for the innermost atoms but become large for the outermost atoms and increase with the TBG size. However, one may expect that the  $\gamma$  value becomes steady for large-sized systems in which the electron accumulation at the QD edge through intralayer conjugation paths, namely, the edge effect [55], reaches its limit. Assuming all atoms in the outermost shells are of  $\gamma_{AB}$  and all the other atoms of  $\gamma_{AA}$  in a moiré period, the interlayer polarizability is derived as

$$\overline{\langle \alpha_{zz}^Q \rangle} = \frac{1}{N_{tot}} \left( \sum_{j=1}^k N_j \gamma_{AA} r_{j,z} + \sum_{j=k+1}^m N_j \gamma_{AB} r_{j,z} \right), \quad (6)$$

where  $j$  is the shell number, and  $m = 1 + 1/\sqrt{8(1 - \cos\theta)}$  is the number of shells in a periodic moiré pattern at a twist angle of  $\theta$ . Here,  $N_j = 12j - 6$  is the number of atoms in shell  $j$ , and  $N_{tot} = \sum N_j$ . Also,  $k$  and  $(m-k)$  are numbers of shells in which all atoms are of  $\gamma_{AA}$  and  $\gamma_{AB}$ , respectively. Further,  $r_{j,z}$  is the  $z$  coordinate of the atoms.



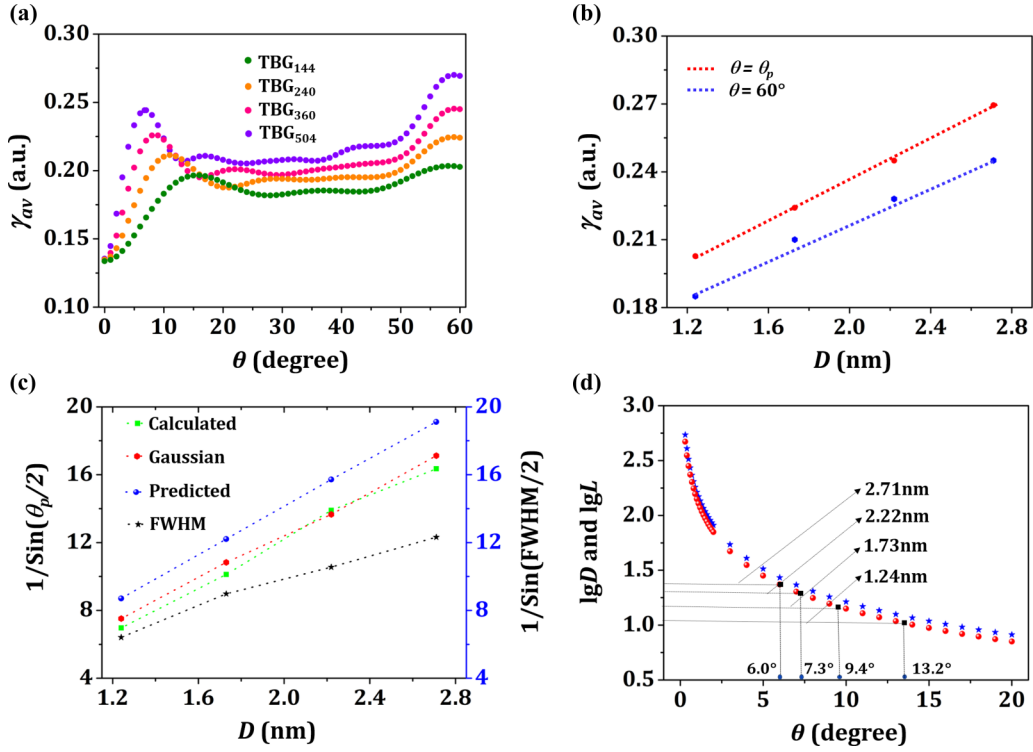


FIG. 4. (a) The computed  $\gamma_{av}$  vs twist angle. (b) Variation of  $\gamma_{av}$  with quantum dot (QD) diameter. The fitted lines are  $\gamma_{av} = 0.0451 D + 0.146$ ,  $R^2 = 0.999$  for the Bernal structures (in red), and  $\gamma_{av} = 0.0404 D + 0.137$ ,  $R^2 = 0.991$  for the structures at  $\theta = \theta_p$  (in blue). (c) Correlation of QD size with twist angle and full width at half maximum (FWHM) of the first peak in  $\alpha_{zz}$ . (d) The minimum diameter ( $D$ , in blue) of twisted bilayer graphene (TBG) QDs with enhanced polarizability at varying twist angles.  $L$  (in red) is the corresponding moiré period.

Bulk TBG contains periodic moiré lattices with an equal mix of AA and AB stackings, while in its QD, the AA/AB ratio varies with the twist angle. Although some rules [56] were suggested to distinguish AA and AB stackings morphologically, it remains an open question as to how many shells can be considered as AB stackings. We assume that the outermost shell and its nearest neighbor are in AB stacking, as shown in Fig. 3(b). The AA structure at  $\theta = 0^\circ$  has the lowest value. An enhanced  $\overline{\alpha_{zz}^Q}$  is obtained when  $\theta$  departs from  $0^\circ$ . A small  $\theta$  leads to a long moiré period in which a small portion of atoms is in AB stacking, resulting in small  $\overline{\alpha_{zz}^Q}$ . We show below that the angle corresponding to the first peak of interlayer polarizability varies with QD size. The AB portion increases with  $\theta$ , and their contribution increases gradually, leading to enhanced  $\overline{\alpha_{zz}^Q}$  values at large  $\theta$ . When one more shell is considered as AB stacking, the increase in  $\overline{\alpha_{zz}^Q}$  is further promoted, as shown in Fig. 3(b).

Figure 1(f) and Eq. (6) not only depict the enhanced interlayer polarizability in TBG QDs but also correlate the QD size with twist angle at which the enhanced polarizability first occurs. Figure 4(a) displays the averaged  $\gamma_{av}$  of all atoms for the four models with varying  $\theta$ , which vary in the same patterns with  $\overline{\alpha_{zz}^Q}$  shown in Fig. 1(f), verifying again the decisive role of  $\gamma_{av}$  in interlayer polarizability. The first peak occurs at a smaller angle for a larger-sized structure. Among the four structures, the peak height increases with size because of the significant edge effect [55] in small-sized systems.

Figure 4(b) indicates a nearly linear increase of  $\gamma_{av}$  with QD diameter. Since the interlayer separation is fixed, this implies that the polarizability is predicted to increase linearly with QD volume, as is seen in other atomic clusters [57]. The enhanced  $\gamma_{av}$  is more significant in small-sized QDs. The first peak of TBG<sub>144</sub> is comparable in height with that of the corresponding Bernal structure, while the height of the first peak of TBG<sub>504</sub> becomes lower than its Bernal stacking. Fitting these first peaks to Gaussians, one has the first peaks at  $15.3^\circ$ ,  $10.6^\circ$ ,  $8.4^\circ$ , and  $6.7^\circ$  for the four QDs, respectively. In another way, since the first peak occurs at the angle where AB stacking first appears in the outermost layer, the diameter of the QD ( $D$ ) and its corresponding twist angle for the first peak can be related as

$$D = \frac{d}{\sin(\frac{\theta}{2})}, \quad (7)$$

where  $d$  is the C-C bond length. Using Eq. (7), the twist angle at which the first peak appears for the four QD models can then be estimated as  $13.2^\circ$ ,  $9.4^\circ$ ,  $7.3^\circ$ , and  $6.0^\circ$ , matching well with the Gaussian-fit angles, as shown in Fig. 4(c). It is apparent that a better agreement can be reached for larger-sized QDs.

Furthermore, the Gaussian-fit full width at half maximum (FWHM) of the first peaks exhibit good correlation with QD size, as shown in Fig. 4(c). In fact, a small  $\Delta\theta$  leads to large displacements of outermost atoms in a large-sized QD, and vice versa. The QD size, twist angle, and FWHM are

interdependent at the first peak of interlayer polarizability. Therefore, it becomes possible to predict the minimum twist angle required for enhanced interlayer polarizability at a given QD size or vice versa. For example, a minimum twist angle of about  $0.54^\circ$  would be predicted for a QD of 30 nm in diameter, and a QD diameter of  $\sim 16.3$  nm would be predicted for an observed  $\theta_p = 1^\circ$ . Figure 4(d) highlights the angle at which the first polarizability peak occurs for the QD with a specified size. All four models studied here find their positions on the curve. The size-angle dependence has also been noted for two graphene flakes [58], a quasiparallelogram with averaged axis of 1.13 nm in length. Strong interlayer coupling was predicted at  $\theta = 15^\circ$ , matching well with the angle of  $14.1^\circ$  predicted using Eq. (7). In fact, the QD size  $D$  is related to the moiré period  $L$  as  $L = \sqrt{3}/2D$ . Figure 4(d) shows the correlation of  $L$  and  $D$  at magic angles where enhanced interlayer polarizability is found. This reveals the direct correlation between the interlayer polarizability and the formation of a moiré pattern in TBG QDs.

#### IV. SUMMARY

In summary, we compute the interpolarizability and intrapolarizability in TBG QDs and demonstrate that there are significant changes in the polarizability as a function of twist angle, dominated by variations in interlayer polarizability, while intralayer polarizability is essentially unchanged. A quantity  $\gamma_{av}$  is defined from interlayer polarizability and used

to measure the interlayer coupling strength. In addition to the large  $\gamma_{av}$  values in the Bernal stackings, enhanced  $\gamma_{av}$  are characterized at small twist angles. These findings indicate an important fact that strong interlayer coupling in TBG QDs occurs not only in the well-recognized Bernal stackings with a large twist angle but also in the structures with small twist angles. Moreover,  $\gamma_{av}$  varies with the structural interplay between AA and AB stackings, and its maxima depend on the appearance of AB stackings and consequently on the size of the sample. An empirical model is proposed to describe the  $\gamma_{av}$  variations. However, it remains a challenge to deduce an accurate model that reflects the  $\gamma_{av}$  variations with interlayer twist, interlayer stacking, and QD size. A correlation between the smallest twist angle and the minimum size for observing polarizability enhancement in finite-sized TBG is derived and verified by the computations with QD models.

In this paper, we develop an approach for the effective measurement of interlayer coupling strength, which is necessary for the precise control of interlayer charge flow in multi-layer graphene. This paper also suggests further exploration on the correlation of interlayer metallicity/dielectricity with other properties enhanced by the formation of moiré pattern in TBG.

#### ACKNOWLEDGMENTS

The authors are grateful for the financial support from the National Natural Science Foundation of China (No. 21773159).

- 
- [1] B. Trauzettel, D. V. Bulaev, D. Loss, and G. Burkard, *Nat. Phys.* **3**, 192 (2007).
- [2] M. Fuchs, J. Schliemann, and B. Trauzettel, *Phys. Rev. B* **88**, 245441 (2013).
- [3] H. Min, J. E. Hill, N. A. Sinitsyn, B. R. Sahu, L. Kleinman, and A. H. MacDonald, *Phys. Rev. B* **74**, 165310 (2006).
- [4] D. Kochan, M. Gmitra, and J. Fabian, *Phys. Rev. Lett.* **112**, 116602 (2014).
- [5] M. Bockrath, *Nano Lett.* **5**, 2937 (2020).
- [6] L. Banszerus, B. Frohn, A. Epping, D. Neumaier, K. Watanabe, T. Taniguchi, and C. Stampfer, *Nano Lett.* **18**, 4785 (2018).
- [7] M. Eich, F. Herman, R. Pisoni, H. Overweg, A. Kurzmann, Y. Lee, P. Rickhaus, K. Watanabe, T. Taniguchi, M. Sigrist, T. Ihn, and K. Ensslin, *Phys. Rev. X* **8**, 031023 (2018).
- [8] C. Volk, S. Fringes, B. Terres, J. Dauber, S. Engels, S. Trellenkamp, and C. Stampfer, *Nano Lett.* **11**, 3581 (2011).
- [9] L. Banszerus, A. Rothstein, T. Fabian, S. Möller, E. Icking, S. Trellenkamp, F. Lentz, D. Neumaier, K. Watanabe, T. Taniguchi, F. Libisch, C. Volk, and C. Stampfer, *Nano Lett.* **20**, 7709 (2020).
- [10] M. Eich, R. Pisoni, A. Pally, H. Overweg, A. Kurzmann, Y. Lee, P. Rickhaus, K. Watanabe, T. Taniguchi, K. Ensslin, and T. Ihn, *Nano Lett.* **18**, 5042 (2018).
- [11] A. Kurzmann, H. Overweg, M. Eich, A. Pally, P. Rickhaus, R. Pisoni, Y. Lee, K. Watanabe, T. Taniguchi, T. Ihn, and K. Ensslin, *Nano Lett.* **19**, 5216 (2019).
- [12] L. A. Gonzalez-Arraga, J. L. Lado, F. Guinea, and P. San-Jose, *Phys. Rev. Lett.* **119**, 107201 (2017).
- [13] M. A. Aamir, P. Karnatak, A. Jayaraman, T. P. Sai, T. V. Ramakrishnan, R. Sensarma, and A. Ghosh, *Phys. Rev. Lett.* **121**, 136806 (2018).
- [14] A. Ramires and J. L. Lado, *Phys. Rev. Lett.* **121**, 146801 (2018).
- [15] R. Battilomo, N. Scopigno, and C. Ortix, *Phys. Rev. Lett.* **123**, 196403 (2019).
- [16] T. M. R. Wolf, J. L. Lado, G. Blatter, and O. Zilberberg, *Phys. Rev. Lett.* **123**, 096802 (2019).
- [17] J. Velasco, J. Lee, D. Wong, S. Kahn, H. Tsai, J. Costello, T. Umeda, T. Taniguchi, K. Watanabe, and A. Zettl, *Nano Lett.* **18**, 5104 (2018).
- [18] H. Overweg, H. Eggimann, X. Chen, S. Slizovskiy, M. Eich, R. Pisoni, Y. Lee, P. Rickhaus, K. Watanabe, and T. Taniguchi, *Nano Lett.* **18**, 553 (2018).
- [19] A. Uri, S. Grover, Y. Cao, J. A. Crosse, K. Bagani, D. Rodan-Legrain, Y. Myasoedov, K. Watanabe, T. Taniguchi, and P. Moon, *Nature (London)* **581**, 47 (2020).
- [20] A. Sagar, E. J. H. Lee, K. Balasubramanian, M. Burghard, and K. Kern, *Nano Lett.* **9**, 3124 (2009).
- [21] V. Perebeinos, J. Tersoff, and Ph. Avouris, *Phys. Rev. Lett.* **109**, 236604 (2012).
- [22] Z. W. Yu, A. S. Song, L. Z. Sun, Y. L. Z. Li, L. Gao, H. L. Peng, T. B. Ma, Z. F. Liu, and J. B. Luo, *Small* **16**, 1902844 (2020).
- [23] S. Zhou, A. S. Song, L. X. Chen, C. X. Jiang, C. Chen, L. Gao, Y. Hong, L. Q. Liu, T. B. Ma, H. M. Wang, X. Q. Feng, and Q. Y. Li, *Sci. Adv.* **6**, eabc5555 (2020).
- [24] Y. Cao, V. Fatemi, S. Fang, K. Watanabe, T. Taniguchi, E. Kaxiras, and P. Jarillo-Herrero, *Nature (London)* **556**, 43 (2018).

- [25] M. Yankowitz, S. Chen, H. Polshyn, Y. Zhang, K. Watanabe, T. Taniguchi, D. Graf, A. Young, and C. Dean, *Science* **363**, 1059 (2019).
- [26] Y. Cao, V. Fatemi, A. Demir, S. Fang, S. L. Tomarken, J. Y. Luo, J. D. Sanchez-Yamagishi, K. Watanabe, T. Taniguchi, E. Kaxiras, R. C. Ashoori, and P. Jarillo-Herrero, *Nature (London)* **556**, 80 (2018).
- [27] G. Li, A. Luican, J. M. B. L. D. Santos, A. H. C. Neto, A. Reina, J. Kong, and E. Y. Andrei, *Nat. Phys.* **6**, 109 (2010).
- [28] A. Kerelsky, L. J. Mcgilly, D. M. Kennes, L. Xian, M. Yankowitz, S. Chen, K. Watanabe, T. Taniguchi, J. Hone, and C. Dean, *Nature (London)* **572**, 95 (2019).
- [29] B. Liu, Y. Sheng, S. Huang, Z. Guo, K. Ba, H. Yan, W. Bao, and Z. Sun, *Chem. Mater.* **31**, 6105 (2019).
- [30] T. Ihn, J. Güttinger, F. Molitor, S. Schnez, E. Schurtenberger, A. Jacobsen, S. Hellmüller, T. Frey, S. Dröscher, C. Stampfer, and K. Ensslin, *Mater. Today* **13**, 44 (2010).
- [31] D. Y. Pan, J. C. Zhang, Z. Li, and M. H. Wu, *Adv. Mater.* **22**, 734 (2010).
- [32] S. Engels, B. Terrés, A. Epping, T. Khodkov, K. Watanabe, T. Taniguchi, B. Beschoten, and C. Stampfer, *Phys. Rev. Lett.* **113**, 126801 (2014).
- [33] L. Wang, I. Meric, P. Y. Huang, Q. Gao, Y. Gao, H. Tran, T. Taniguchi, K. Watanabe, L. M. Campos, D. A. Muller, J. Guo, P. Kim, J. Hone, K. L. Shepard, and C. R. Dean, *Science* **342**, 614 (2013).
- [34] Y. P. Yang, J. D. Li, J. Yin, S. G. Xu, C. Mullan, T. Taniguchi, K. Watanabe, A. K. Geim, K. S. Novoselov, and A. Mishchenko, *Sci. Adv.* **6**, eabd3655 (2020).
- [35] Y. Jiang, X. Lai, K. Watanabe, T. Taniguchi, K. Haule, J. Mao, and E. Y. Andrei, *Nature (London)* **573**, 91 (2019).
- [36] R. Bistritzer and A. H. MacDonald, *Phys. Rev. B* **81**, 245412 (2010).
- [37] B. Sahu, H. Min, A. H. MacDonald, and S. K. Banerjee, *Phys. Rev. B* **78**, 045404 (2008).
- [38] J. Shen, Y. Zhu, X. Yang, and C. Li, *Chem. Commun.* **48**, 3686 (2012).
- [39] M. J. Frisch, G. W. Trucks, H. B. Schlegel, G. E. Scuseria, M. A. Robb, J. R. Cheeseman, G. Scalmani, V. Barone, G. A. Petersson, H. Nakatsuji *et al.*, *Gaussian 16, Revision C.01* (Gaussian, Inc., Wallingford, CT, 2016).
- [40] T. Yanai, D. Tew, and N. A. Handy, *Chem. Phys. Lett.* **393**, 51 (2004).
- [41] J. -D. Chai and M. Head-Gordon, *Phys. Chem. Chem. Phys.* **10**, 6615 (2008).
- [42] M. J. Frisch, J. A. Pople, and J. S. Binkley, *J. Chem. Phys.* **80**, 3265 (1984).
- [43] H. D. Cohen and C. C. J. Roothaan, *J. Chem. Phys.* **43**, S034 (1965).
- [44] F. L. Hirshfeld, *Theor. Chim. Acta.* **44**, 129 (1977).
- [45] B. Rousseau, A. Peeters, and C. Van Alsenoy, *Chem. Phys. Lett.* **324**, 189 (2000).
- [46] See Supplemental Material at <http://link.aps.org/supplemental/10.1103/PhysRevB.104.155411> for the relative energy, equilibrium interlayer distance of TBG<sub>144</sub> rotating about one of the C atoms in the central six-membered ring, and the total polarizability of TBG<sub>144</sub>, TBG<sub>240</sub>, TBG<sub>360</sub>, and TBG<sub>504</sub> when interlayer rotation is about the hexagonal center.
- [47] H. Shi, Z. Zhan, Z. Qi, K. Huang, E. Van Veen, J. A. Silvaguillen, R. Zhang, P. Li, K. Xie, and H. Ji, *Nat. Commun.* **11**, 371 (2020).
- [48] M. J. Park, Y. Kim, G. Y. Cho, and S. B. Lee, *Phys. Rev. Lett.* **123**, 216803 (2019).
- [49] K. Jackson, M. Yang, and J. Jellinek, *J. Phys. Chem. C.* **111**, 17952 (2007).
- [50] K. Jackson and J. Jellinek, *J. Chem. Phys.* **145**, 244302 (2016).
- [51] L. Ma, K. A. Jackson, J. Wang, M. Horoi, and J. Jellinek, *Phys. Rev. B* **89**, 035429 (2014).
- [52] K. Jackson, L. Ma, M. Yang, and J. Jellinek, *J. Chem. Phys.* **129**, 144309 (2008).
- [53] R. Nashed, C. Y. Pan, X. Y. Wu, I. Asselberghs, Z. Tokei, F. Cathoor, and A. Naeemi, *IEEE T. Electron. Dev.* **67**, 627 (2020).
- [54] Y. L. Han, J. J. Zeng, Y. F. Ren, X. L. Dong, W. Ren, and Z. H. Qiao, *Phys. Rev. B* **101**, 235432 (2020).
- [55] D. Bischoff, A. Varlet, P. Simonet, M. Eich, H. C. Overweg, T. Ihn, and K. Ensslin, *Appl. Phys. Rev.* **2**, 031301 (2015).
- [56] K. Uchida, S. Furuya, J. I. Iwata, and A. Oshiyama, *Phys. Rev. B* **90**, 155451 (2014).
- [57] M. L. Yang, K. A. Jackson, and J. Jellinek, *J. Chem. Phys.* **132**, 064306 (2010).
- [58] J. Berashevich and T. Chakraborty, *Phys. Rev. B* **84**, 033403 (2011).